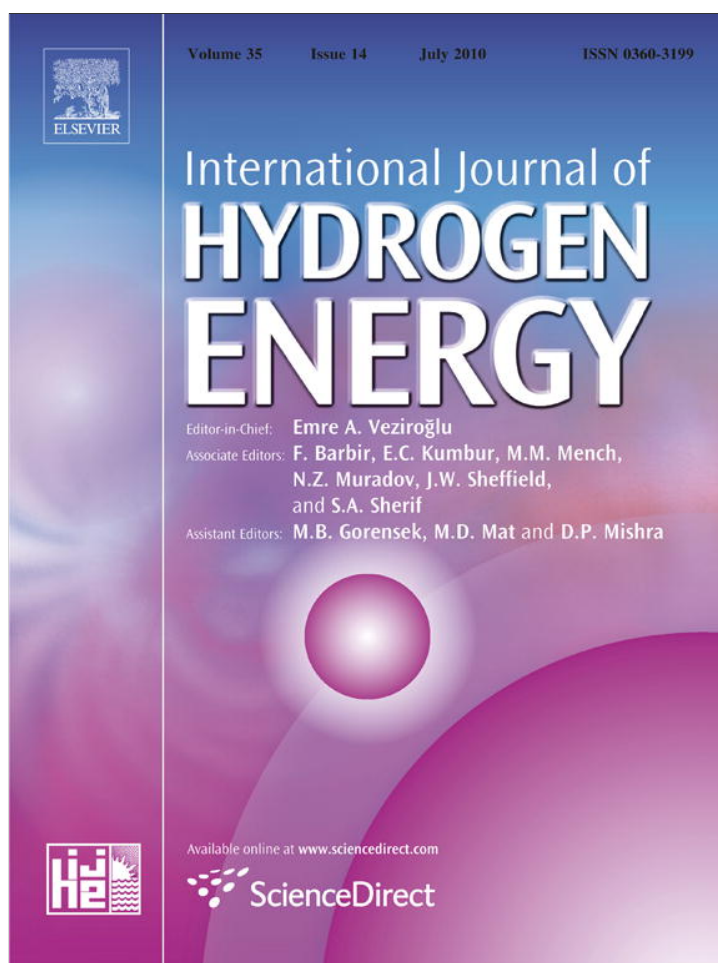


Provided for non-commercial research and education use.
Not for reproduction, distribution or commercial use.

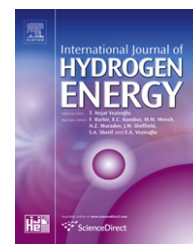


This article appeared in a journal published by Elsevier. The attached copy is furnished to the author for internal non-commercial research and education use, including for instruction at the authors institution and sharing with colleagues.

Other uses, including reproduction and distribution, or selling or licensing copies, or posting to personal, institutional or third party websites are prohibited.

In most cases authors are permitted to post their version of the article (e.g. in Word or Tex form) to their personal website or institutional repository. Authors requiring further information regarding Elsevier's archiving and manuscript policies are encouraged to visit:

<http://www.elsevier.com/copyright>

Available at www.sciencedirect.comjournal homepage: www.elsevier.com/locate/he

Catalytic decomposition of liquid hydrocarbons in an aerosol reactor: A potential solar route to hydrogen production

Xiaofei Ma, Anshuman A. Lall¹, Natan Aronhime, Michael R. Zachariah*

Department of Chemistry and Biochemistry, and Mechanical Engineering, University of Maryland-College Park, MD, USA

ARTICLE INFO

Article history:

Received 21 February 2010

Received in revised form

27 April 2010

Accepted 2 May 2010

Available online 2 June 2010

Keywords:

Thermal decomposition

Liquid hydrocarbons

Aerosol reactor

Iron catalyst

Hydrogen energy

ABSTRACT

Catalytic decomposition of liquid fuels (n-octane, iso-octane, 1-octene, toluene and methylcyclohexane) is achieved in a continuous tubular aerosol reactor as a model for the solar initiated production of hydrogen, and easily separable CO free carbonaceous aerosol product. The effects of fuel molecular structure and catalyst concentration on the overall hydrogen yield were studied. Iron aerosol particles used as the catalysts, were produced on-the-fly by thermal decomposition of iron pentacarbonyl. The addition of iron catalyst significantly decreases the onset temperature of hydrogen generation as well as improves the reaction kinetics by lowering the reaction activation energy. The activation energy without and with iron addition was 260 and 100 kJ/mol, respectively representing a decrease of over 60%. We find that with the addition of iron, toluene exhibits the highest hydrogen yield enhancement at 900 °C, with a 6 times yield increase over thermal decomposition. The highest H₂ yield obtained was 81% of the theoretical possible, for n-octane at 1050 °C. The general trend in hydrogen yield enhancement is that the higher the non-catalytic thermal decomposition yield, the weaker the catalytic enhancement. The gaseous decomposition products were characterized using a mass spectrometer. An XRD analysis was conducted on the wall deposit to determine the product composition and samples for electron-microscopic analysis were collected exiting the furnace by electrostatically precipitating the aerosol onto a TEM grid.

© 2010 Professor T. Nejat Veziroglu. Published by Elsevier Ltd. All rights reserved.

1. Introduction

Any realization of hydrogen economy depends on the availability of large quantities of hydrogen produced at low cost. The hydrogen economy is environmental-friendly only when the production of hydrogen is CO₂ free. Currently, hydrogen is produced mainly through steam reforming of natural gas followed by the water gas shift reaction of CO [1]. The reaction is highly endothermic, and hence requires a substantial energy input. Furthermore, the water gas shift reaction is a major source of industrial CO₂. If the CO₂ by-product cannot

be fully used or sequestered, the environmental gain from using hydrogen as an alternative fuel to hydrocarbons is largely lost. One of the hydrogen production methods that can address these two issues simultaneously is thermal decomposition of hydrocarbons into hydrogen and carbon [2–4]. It provides an alternative, one-step process to produce hydrogen of the required purity. The process is oxygen free thus produces no oxidative products CO/CO₂. This feature is important to polymer electrolyte membrane (PEM) fuel cells since PEM fuel cells require hydrogen with very low CO concentration (<10 ppm). Currently, a multiple-step process is

* Corresponding author. Tel.: +1 301 405 4311; fax: +1 301 314 9477.

E-mail address: mrz@umd.edu (M.R. Zachariah).

¹ Present address: Excet, Inc., Springfield, VA, USA.

required to produce high purity hydrogen which involves steps to produce synthesis gas, water gas shift reactions to convert CO to CO₂ and H₂, and various purification steps to reduce the CO to ppm levels. Compared with that, the H₂ separation in the thermal decomposition process is relatively easy since the major carbon product is in solid phase. The solid carbons are easier to separate, handle, transport and store than gaseous CO₂ and the product hydrogen can be supplied directly to PEM fuel cells. If taken to completion, the by-product of the decomposition could be tuned to produce valuable carbon products such as carbon black, carbon nanotubes or carbon filaments. Because of these attractive advantages of thermal decomposition, there is an increasing interest in this area. However, most studies have addressed the decomposition of methane. From a thermodynamic point of view, the decomposition of liquid hydrocarbons is favored over methane since 1.5–2 times less energy is needed to produce a unit volume of hydrogen [5]. From a practical point of view, decomposition of liquid fuel is more suitable for onboard hydrogen generation, since the current transportation, storage and dispersal infrastructure for gasoline can be easily modified for other liquid fuels. Finally, methane combustion produces the lowest GWP products since it is a hydrocarbon with highest fraction of hydrogen.

Sunlight provides by far the largest of all carbon-neutral energy sources. Basically, three pathways have been identified for producing hydrogen using solar energy [6]. They are electrochemical, photochemical, and thermochemical. The last method uses concentrated solar radiation as the energy source of high-temperature process heat for chemical transformations. Modern solar-concentrating systems can achieve maximum concentration factors in the 1500–5000 range and provide high-temperature solar thermal heat exceeding 2000 °C, thus capable of driving very endothermic chemical reactions. Various solar thermochemical routes have been proposed, and implemented on a solar reactor. For example, Zn/ZnO redox pair [7,8] is considered as one of the most favorable candidates for 2-step water-splitting thermochemical cycle for hydrogen production. The first step of the cycle, which is the solar dissociation of ZnO, has been carried out successfully in solar furnaces at high-temperatures (>1500 K) [9,10]. Solar thermochemical decarbonization of hydrocarbons is also a promising approach. Solar furnaces and reactors have been employed to study the decomposition of gaseous hydrocarbons [11–13] such as methane and butane for the catalytic production of hydrogen and filamentous carbon. Dahl et al. [11]. Designed a solar tubular quartz reactor containing fine carbon black particles suspended in a CH₄ feed gas stream, with a dissociation up to 90% at 2133 K. Steinfeld [14] and his co-worker designed a solar chemical reactor which features a vortex flow of CH₄ confined to a cavity-receiver and laden with carbon particles that serve simultaneously as radiant absorbers and nucleation sites for the heterogeneous decomposition reaction. A maximum chemical conversion of CH₄ to H₂ and C was 67% at 1600 K and 1 bar. However both these approaches use methane which is itself a highly valued fuel which is high in hydrogen. Combustion of liquid hydrocarbons is more deleterious to the environment because of their lower hydrogen content. On the other hand, given that the decomposition of liquid fuels requires less energy than the

decomposition of methane, solar thermal process employing liquid hydrocarbons should achieve higher conversion rates. Even more so if catalytic process enhance the decomposition rate or conversion efficiency at a given temperature.

We begin by discussing prior relevant work on liquid fuel thermal decomposition. Otsuka et al. [15] examined the decomposition of various alkanes over Ni/fumed silica catalysts at 773 K. Hydrogen and carbon nanofilaments were found as the major products with a low concentration of methane. The authors concluded that gasoline range alkanes (C₆-alkane, C₈H₁₈) were superior to the light alkanes (<C₄) for selective decomposition into hydrogen and carbon. Takenaka et al. [16] investigated the decomposition of various hydrocarbons (propane, n-butane, n-hexane, cyclohexane, toluene and n-octane) using a conventional gas flow system with a fixed catalyst bed over Ni based catalysts. They concluded that the saturated hydrocarbons could be a promising feedstock for hydrogen generation.

Metals (ions, atoms, clusters) are known to have a catalyst effect on the activation of carbon–carbon and carbon–hydrogen bonds in hydrocarbons. Transition and noble metal catalysts such as Ni, Fe, Cu, Co, Pt, Rh, Pd supported on high surface area ceramic substrates such as Al₂O₃ and SiO₂, have been investigated in the decomposition process of gaseous and liquid hydrocarbons [5]. Other novel catalyst and support materials have also been investigated for liquid fuel decomposition. For example, Ichikawa et al. [17,18] investigated the dehydrogenation of cyclohexane, methylcyclohexane and decalin over activated carbon supported Ni, Pt, and Ni–Pt catalysts at 287–375 °C. A conversion between 25 and 35% was found with the selectivity for dehydrogenation reactions above 98.8%. Okada et al. [19] developed a unimodal porous alumina supported dehydrogenation catalyst which yielded 95% methylcyclohexane conversion and give a 38% of theoretical H₂ yield, with the primary product toluene. Wang et al. [20] used stacked-cone carbon nanotubes as a support to prepare Pt and Pd catalysts for the dehydrogenation of cyclohexane and methylcyclohexane, and later reported results [21] of alumina supported nano-scale binary catalysts for propane and cyclohexane decomposition. The catalyst has been shown to be very effective for the decomposition of lower alkanes to produce hydrogen and carbon nanofibers or nanotubes. The decomposition of Jet A mixture, cyclohexane, decalin were performed [22] over a hybrid catalyst, Pt/γ-Al₂O₃–ZrO₂/SO²⁻. The acidity of the catalyst promote the cracking ability but also promotes coke formation and thus to rapid deactivation of the catalyst. The major challenges remaining in the catalyst development for decomposition are coking prevention, and performance enhancement. The majority of the studies were performed using conventional fixed-bed reactors with few using other reactor configurations.

In this study, we employ an aerosol reactor to study the decomposition of liquid fuels with emphasizes on the effect of fuel molecular structure on the hydrogen yield. The uniqueness of the work comes from conducting the decomposition over aerosol catalyst and producing hydrogen and carbonaceous aerosol. In this work catalyst iron nanoparticles were generated in-situ, and are in the aerosol state, thus can maximize the contact area between the fuel and the catalyst

Table 1 – Physical properties of the fuels investigated.

	Density at 25 °C (g/ml)	Purity (%)	Vapor Pressure (torr)	Melting Point (°C)	Boiling Point (°C)
n-octane	0.703	98	11 (20 °C)	–57	125–127
iso-octane	0.692	>99	41 (21 °C)	–107	98–99
1-octene	0.715	98	15 (20 °C)	–101	122–123
toluene	0.865	>99.5	22 (20 °C)	–93	110–111
methylcyclohexane	0.77	99	37 (20 °C)	–126	101

particles. With this approach the catalyst is a one time use, and thus poisoning is not so great a concern and as such we can drive the chemistry harder. However, this approach necessarily requires that the catalyst material be inexpensive, and the use of precious metals or complex mixtures would not be considered practical. Thus the choice of iron. A second and equally important aspect of this approach is that the hydrogen product is CO₂ free and easily separated from the other product of decomposition, carbonaceous aerosol.

2. Experimental

The catalytic decomposition of liquid fuels was performed in an aerosol reactor with a controlled gas flow system. Iron nanoparticle catalysts were generated on-the-fly by thermally decomposition of iron pentacarbonyl.

Previous studies by Karlsson et al. on iron carbonyl thermal decomposition [23] found that it was difficult to regulate the iron pentacarbonyl vapor flow because of its high volatility. To mitigate this problem we mixed the iron carbonyl directly into the liquid fuel and then bubbled argon through the mixture. The vapor composition is determined by the molar ratio of the two components according to Raoult's law.

The advantage of this approach is that due to the lower decomposition temperature of the iron carbonyl we initiate the catalyst production just prior to the initiation of the hydrocarbon decomposition chemistry. This minimizes the growth rate of the particles and thus maximizes surface area.

The aerosol reactor consists of a 22 mm I.D. 25 mm O.D. quartz tube within a 30 cm heated length, and with a nominal residence time of ~1 min. The gaseous product was characterized by a mass spectrometer (Stanford Research UGA 300) which also monitored the hydrogen and argon partial pressures with time. Argon was used as an inert internal standard and to determine the volume change of gaseous reactants and products during the reaction so as to assign concentrations. The mass of the fuel was measured each time before and after the experiment to calculate the fuel consumption rate. Samples for electron-microscopic analysis were collected by electrostatically precipitating the aerosol onto a TEM grid using an electrostatic precipitator. Since a lot of materials were deposited on the wall of the quartz reactor tube, XRD analysis was employed to determine the composition of the wall deposit.

To study the effect of fuel molecular structure on the overall hydrogen conversion, different types of hydrocarbon fuels were selected according to the classification: saturated hydrocarbons, unsaturated hydrocarbons, cycloalkanes and aromatic hydrocarbons. N-octane (Sigma–Aldrich, reagent

grade, 98%) was used in the experiment as a representing straight-chain saturated hydrocarbon. Iso-octane (also named 2,2,4-Trimethylpentane, Sigma–Aldrich, ACS spectrophotometric grade, ≥99%) was selected to investigate the chain branching effect of alkanes. 1-octene (Sigma–Aldrich, 98%) was chosen as the representing unsaturated hydrocarbon with one carbon–carbon double bond. Toluene (EMD, >99.5%)

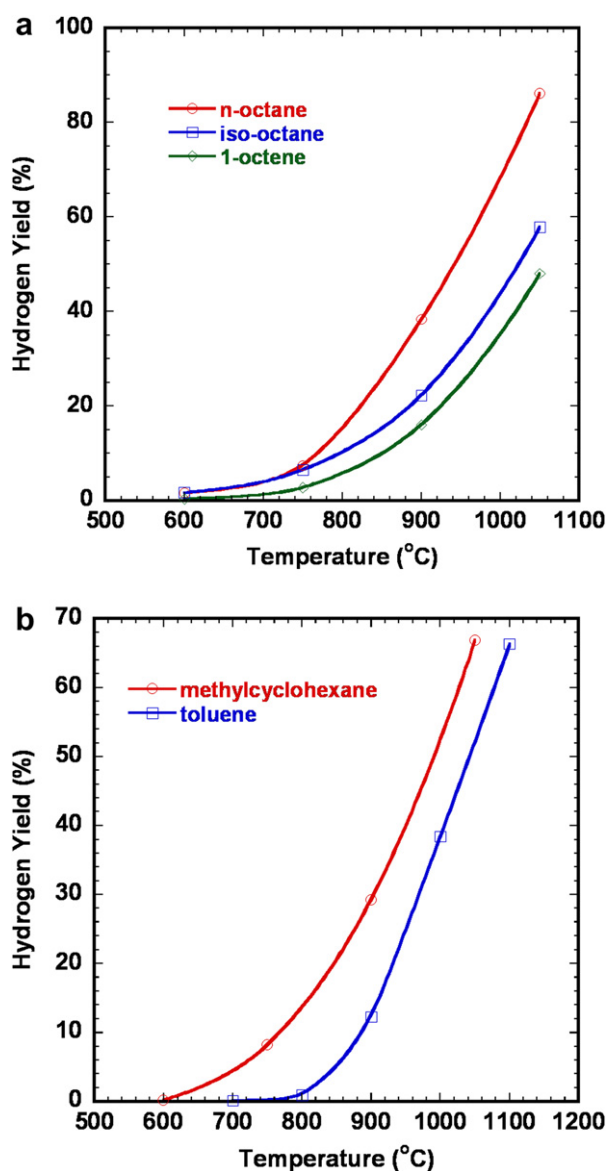


Fig. 1 – Hydrogen yields from thermal decomposition of fuels (a) hydrogen yields from n-octane, iso-octane and 1-octene (b) hydrogen yields from methylcyclohexane and toluene.

Table 2 – C–H bond types in n-octane, iso-octane and 1-octene.

	Number of primary C–H bond (bond dissociation energy 410 kJ/mol)	Number of secondary C–H bond (bond dissociation energy 397 kJ/mol)	Number of tertiary C–H bond (bond dissociation energy 389 kJ/mol)	Number of H–C=C bond (bond dissociation energy 460 kJ/mol)
n-octane	6 (33.3% of the total C–H bonds)	12 (66.7% of the total C–H bonds)	0	0
iso-octane	15 (83.3% of the total C–H bonds)	2 (11.3% of the total C–H bonds)	1 (5.3% of the total C–H bonds)	0
1-octene	3 (18.75% of the total C–H bonds)	10 (62.5% of the total C–H bonds)	0	3 (18.75% of the total C–H bonds)

was used as the representing aromatic hydrocarbon and methylcyclohexane (Sigma–Aldrich, ReagentPlus, 99%) which differs with toluene only in the benzene ring was selected as the representing cycloalkane. The physical properties of the fuels are listed in Table 1.

3. Results and discussion

3.1. Hydrogen yield from thermal decomposition of different liquid fuels

To investigate the effect of fuel molecular structure on the hydrogen generation, thermal decomposition of different hydrocarbons were performed under the same experiment condition, and hydrogen yield for each fuel were calculated as a function of decomposition temperature based on the following equation:

$$Y_{H_2} = \frac{X_{H_2} V_{in} Z_{expansion}}{a \cdot V_{1mole} \cdot r_{fuel,in}}$$

where Y_{H_2} is the hydrogen yield, X_{H_2} is the hydrogen mole fraction in the gaseous product, V_{in} is the input flow rate, $Z_{expansion}$ is the gaseous expansion factor determined from the change of argon partial pressure, a is the stoichiometric factor for complete conversion of a particular fuel to hydrogen, V_{1mole} is the volume of 1 mole ideal gas at room temperature and $r_{fuel,in}$ is the fuel injection rate in moles per minute, which was determined by measuring the mass change of the liquid fuel before and after each experiment run. Using the above equation, the hydrogen yields from pure thermal decomposition of different liquid hydrocarbons were calculated and shown in Fig. 1.

As we can see from the plots, except for toluene, all other fuels start to release hydrogen at around 600 °C. For toluene, the onset temperature of hydrogen generation is about 800 °C, which reflects the greater stability of aromatic structures. The general trend of ease of thermal decomposition is alkanes > alkenes and cycloalkanes > aromatics. Compared with the three fuels in Fig. 1(a), (These fuels have the same carbon number and differ only in the carbon skeleton and bond order) n-octane has the highest hydrogen yield and both n-octane and iso-octane outperform their alkene counterpart (1-octene) in terms of hydrogen yield. However, different from the thermal cracking in petrochemical industry, where branched hydrocarbons are always found to be more reactive than their straight-chain counterparts [24], the straight-chain

n-octane outperforms its branched-chain counterpart (iso-octane) in hydrogen production. Since carbon–carbon bond scission is the principal reaction during cracking, while hydrogen generation is more related to the C–H bond strength, a comparison of the C–H bond configurations in the three fuels may reveal some insights about trend in overall hydrogen yield. Table 2 shows the number of each C–H bond type, bond dissociation energy, and the percentage of total C–H bonds in n-octane, iso-octane and 1-octene molecules. Clearly, iso-octane has the highest percentage of C–H primary bonds, and n-octane has the highest percentage of secondary C–H bonds. Even though iso-octane has one tertiary C–H bond which is the easiest to dissociate, the fact that the majority of C–H bonds in iso-octane are primary C–H bonds means it's harder to decompose than n-octane. As for 1-octene, the existence of three H–C=C bonds makes it extremely hard to decompose since the hydrogen atom attached to the C=C double bond has much higher bond dissociation energy (460 kJ/mol).

The comparison between toluene and methylcyclohexane is straight forward. Since the dehydrogenation product of toluene is methylcyclohexane, and this reaction is highly endothermic (The heat of reaction is around 205 kJ/mol [19]). Toluene is clearly harder to decompose. As we can see from Fig. 1(b), not only the onset temperature of hydrogen generation for toluene is higher than that of methylcyclohexane, but also the hydrogen yield from toluene is lower than that of methylcyclohexane at all decomposition temperatures.

The order of overall hydrogen yield from thermal decomposition of different fuels follows: n-octane > methylcyclohexane > iso-octane > 1-octene > toluene. As a tentative explanation, the observed hydrogen yield order is compared with the fuel cetane number which characterizes the fuel ignition delay property. Table 3 lists the cetane

Table 3 – Fuel cetane number.

Fuels	Fuel Cetane Number ^a
n-octane	63.8, 64.4, 65
Methylcyclohexane	20, 23
iso-octane	12, 14, 17.5
Toluene	5, 9, 18.3
1-octene	40.5, 41

^a The different values of fuel cetane number are obtained by using different methods.

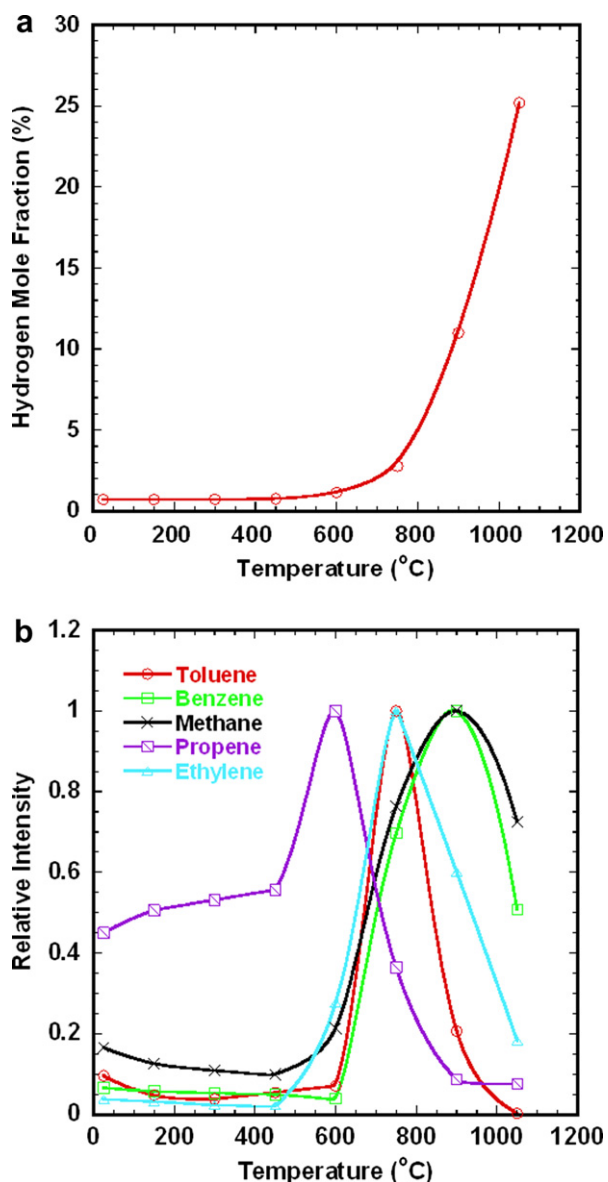


Fig. 2 – Product concentration from n-octane decomposition as a function of decomposition temperature (a) hydrogen mole fraction (b) relative intensities for other gas species.

numbers for fuels investigated in this study. As we can see from the table, except for 1-octene, the larger the cetane number, the higher the hydrogen yields from thermal decomposition. The cetane number characterizes the ease of ignition for a given fuel.

3.2. Gaseous products from thermal decomposition of liquid fuels

Mass spectrums of thermal decomposition product were taken at each reaction temperature using the quadruple mass analyzer. The common decomposition products for all the fuels were hydrogen, toluene, benzene, and methane. For n-octane, the product also contained C2 and C3 olefins; for iso-octane, the product contained C2–C6 olefins; for 1-octene, the

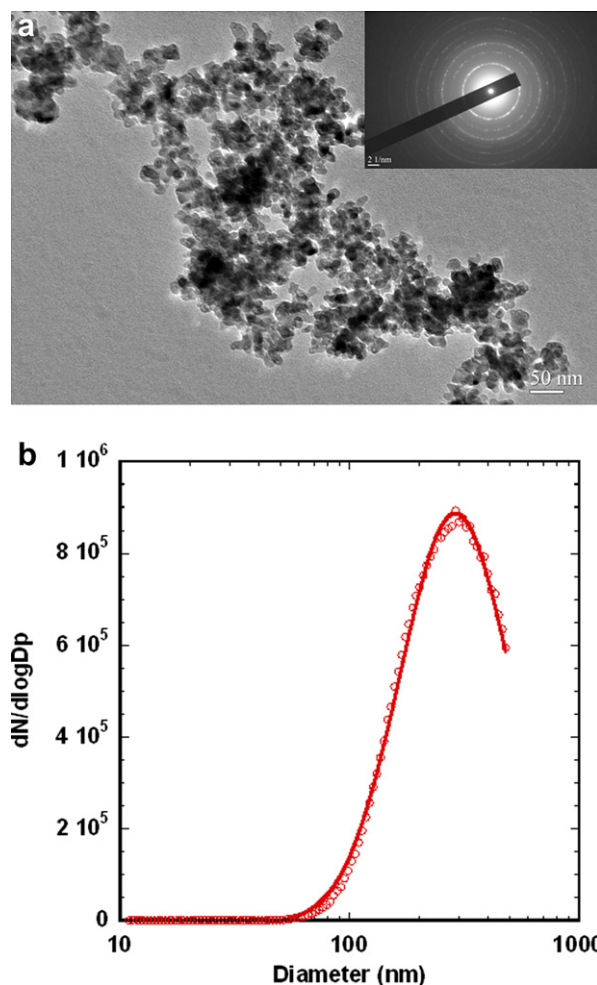


Fig. 3 – (a) TEM image of iron nanoparticle aggregates produced by decomposition of $\text{Fe}(\text{CO})_5$ at 300 °C. (b) Particle size distribution of iron nanoparticle aggregates measured by SMPS.

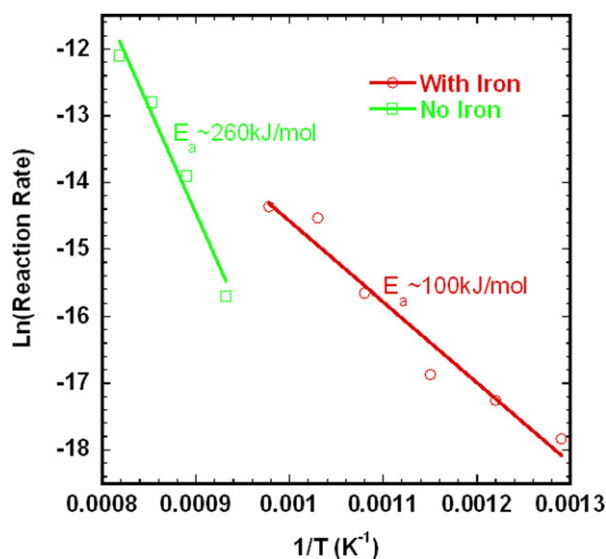


Fig. 4 – Activation energy for toluene decomposition with and without iron addition.

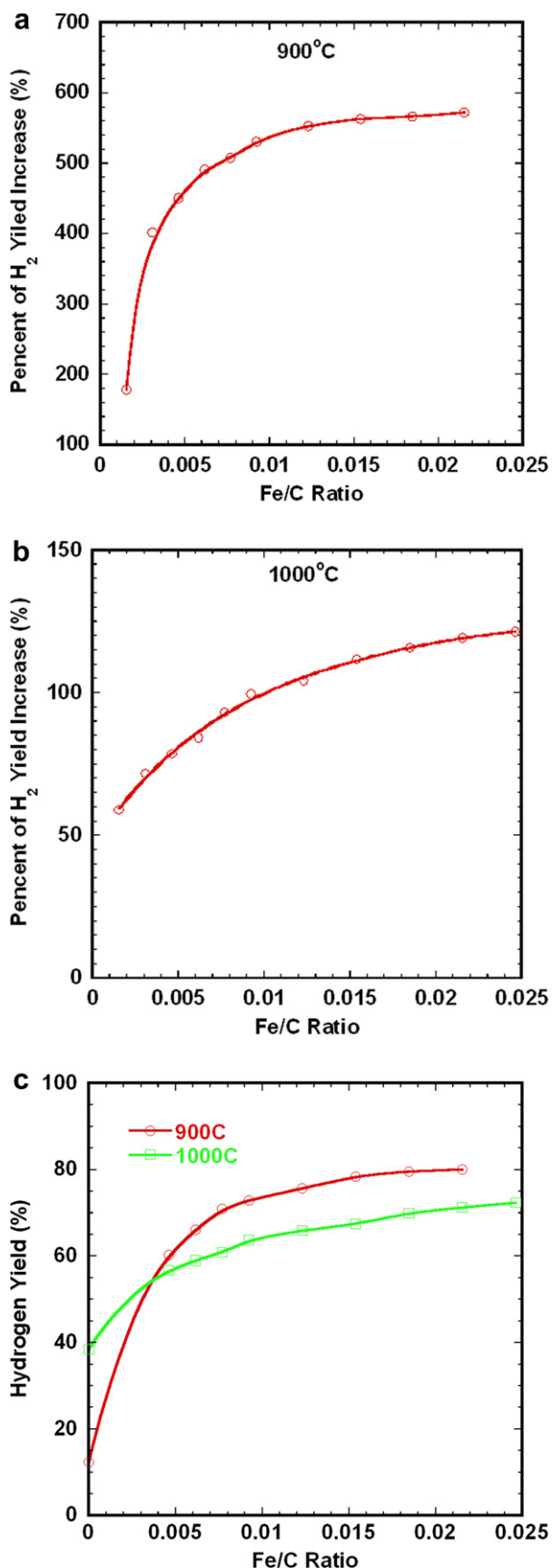


Fig. 5 – Adding water together with fuel and iron precursor greatly enhances the catalytic effect of iron nanoparticles in decomposition of toluene (a) percent of hydrogen yield

product had C2–C3 olefins and alkynes; for methylcyclohexane, the product had C2–C3 olefins and paraffins and for toluene, the product contained C2–C6 paraffins. The similarity in gaseous products from different fuels suggests that at high-temperatures, it is the stability of each gas species that determines the product distribution. Fig. 2(a) and (b) shows species concentration from n-octane decomposition as a function of decomposition temperature. From these plots, we can obtain some qualitative insights into the mechanism of fuel decomposition.

As we can see from the plot, hydrogen partial pressure starts to increase at ~ 600 °C accompanying by the increases in concentration of toluene, methane, ethylene and other gas species. The cracking of the fuel molecule is believed to be initiated by carbon–carbon bond homolysis reaction with the formation of two radicals. The intermediate radicals may undergo carbon–carbon bond homolysis (β -scission) to form olefins (ethylene and propene) and a new radical [25,26]. A stepwise dehydrocyclization with gradual loss of hydrogen to form a conjugated triene followed by ring closure and further dehydrogenation may account for aromatics formation [25]. Therefore, toluene and benzene are produced from their cycloalkane precursors. Studies have shown that the conversion efficiency for preparing toluene from its precursor is nearly 100%, while for benzene this efficiency is lower [25]. At higher temperatures, toluene hydrodealkylation reaction converts toluene to benzene. As Fig. 2(b) shows, toluene concentration peaks at 750 °C, while benzene concentration peaks at 900 °C. At even higher temperatures, benzene decomposition reaction takes over the benzene formation reaction. Methane due to its high stability peaks at 900 °C followed by ethylene at 750 °C, and propene peaks at 600 °C. The decrease in temperature for the peak concentration from methane to ethylene reflects the decrease in thermal stability also reflects the hierarchy of decomposition from larger to smaller molecules.

3.3. Catalytic decomposition of liquid fuels

Metal atoms are believed to have an impact on the activation of carbon–hydrogen and carbon–carbon bonds in hydrocarbons. Reactions initiated by addition of metal atoms across a C–H or C–C bond, results in loss of molecular hydrogen and small alkanes to yield metal ion–olefin complexes. Transition metals are shown to have higher potential in catalyzing this reaction. In our experiment, we produced catalytic iron nanoparticles on-the-fly by thermally cracking the iron pentacarbonyl precursor as discussed in the experimental section. TEM image of the as-produced iron particles are presented in Fig. 3(a) and shows that the primary particles are 10–20 nm in diameter, with electron diffraction confirming elemental iron. The particle size distribution of the catalytic iron particles was measured using an SMPS (scanning mobility particle sizer) system and is presented in Fig. 3(b). The results show that the

increase at 900 °C (b) percent of hydrogen yield increase at 1000 °C (c) absolute hydrogen yield for catalytic toluene decomposition (the data points on the y-axis corresponding to toluene thermal decomposition without catalysts).

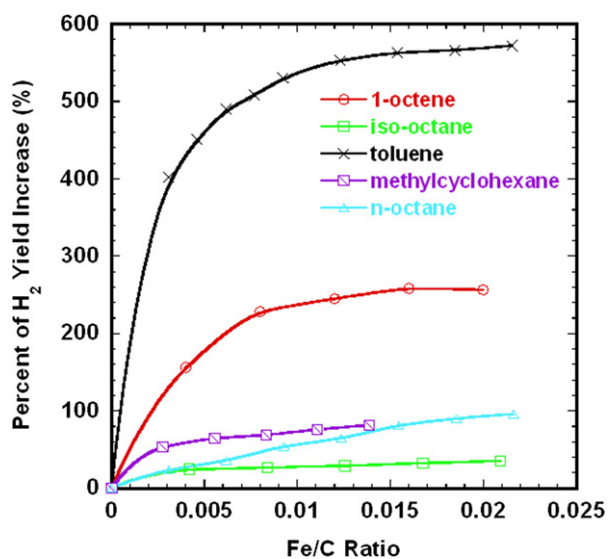


Fig. 6 – Comparison of percent increase of hydrogen yield with iron catalyst concentration for different fuels decomposition at 900 °C.

aggregate sizes are quite large with a median diameter around 300 nm. A large aggregate is actually beneficial in this case, since it should better represent large iron flakes that could be produced by mechanical milling methods if this approach were to be used in an industrial setting. Fig. 4 compares the changes in reaction activation energy for toluene decomposition with and without iron catalysts.

The addition of iron catalyst can significantly lower the onset temperature of hydrogen generation (from ~800 °C to ~600 °C) and decreases the reaction activation energy. However, there is only very limited enhancement in hydrogen

yield. Similar results have been obtained for other fuels. This behavior is well-known and resulted from the coking of catalyst particles since large quantity of solid carbon is produced. To prevent coking and promote the decomposition reaction, a small quantity of water vapor (as a weak oxidizer) was added (several thousand ppm) together with fuel and iron pentacarbonyl during the toluene decomposition. The effect of water addition is presented in Fig. 5.

The addition of water significantly enhances the catalytic power of iron. As we increase the iron loading, the hydrogen yield also increases. An enhancement of 6 times in hydrogen yield was observed at 900 °C with Fe/C ratio of ~0.015. Further increase in iron loading does not increase the hydrogen yield. An interesting result is that the hydrogen yield increase at 1000 °C is not as high as that at 900 °C. A possible reason may be that at higher temperatures the thermal pyrolysis chemistry as well as possible coking of the catalyst competes with catalytic decomposition to minimize the gains of using a catalyst. To compare the catalytic effects, catalytic decomposition of different hydrocarbon fuels were investigated at 900 °C under the same experimental condition. The results are presented in Fig. 6. As we can see from the plot, toluene shows the highest yield enhancement while iso-octane has the weakest enhancement. The general trend in hydrogen yield enhancement can be summarized as: the higher the non-catalytic thermal decomposition yield, the weaker the catalytic enhancement.

3.4. Solid carbon from fuel decomposition

One of the advantages of this process is that the by-product of reaction ideally would be solid carbon and thus separation from hydrogen becomes, from a practical point of view, much simpler. To characterize the carbon particles produced from fuel decomposition, samples for electron-microscopic

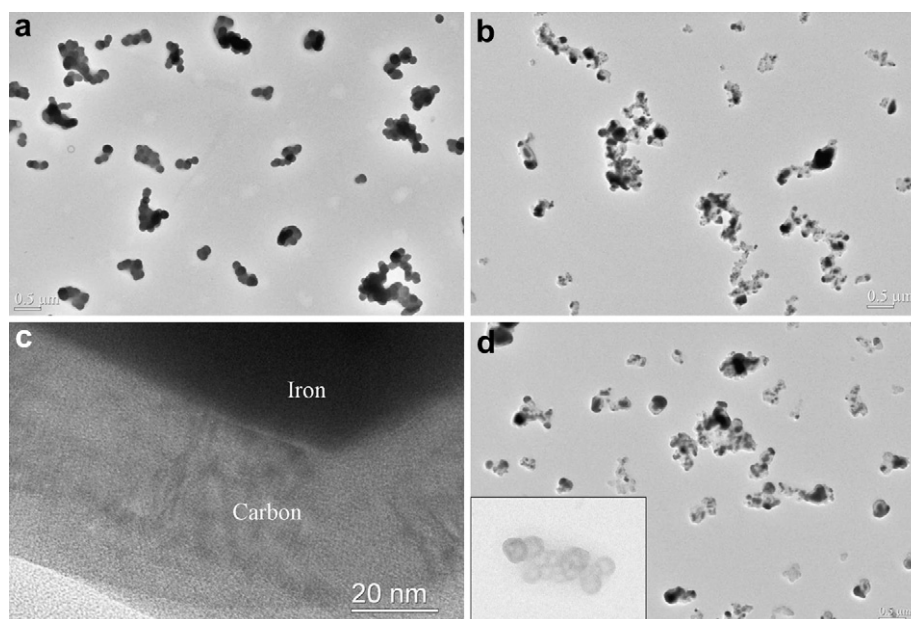


Fig. 7 – Carbon black particles from toluene decomposition under various conditions (a) decomposition at 1000 °C without catalysts, (b) and (c) decomposition at 1000 °C with addition of iron catalysts only, (d) decomposition at 1000 °C with addition of iron catalysts and water vapor.

analysis were collected exiting the reactor by electrostatically precipitating the aerosol onto a TEM grid. Fig. 7 presents the TEM images of carbon black particles collected from toluene decomposition under various experimental conditions. As shown in Fig. 7(a), the particulate products are quite large, about 1 μm in size with primary particle diameters ~ 100 – 130 nm. This is much larger than combustion generated carbon black or soot particles, where primarily particle sizes are nominally under 30 nm. This difference reflects that fact that soot nominally experiences a much higher temperature and thus greater dehydrogenation. In turn, the more graphitic like the particle, the less they sinter, and thus the smaller the resulting primary particles. Fig. 7(b) and (c) show the particle morphology resulting from toluene decomposition at 1000 $^{\circ}\text{C}$ with the addition of iron catalyst only. The darker area within a particle aggregate is iron, while the lighter-colored area is determined to be carbon. A high-resolution image (Fig. 7(c)) shows the crystalline structure of the carbon materials. As we co-inject water vapor together with iron catalysts, hollow carbon particles were observed (shown in Fig. 7(d)) as a result of partial oxidation of carbon particles

by water vapor. The formation of hollow carbon particles also verifies that water vapor as a weak oxidizer, has an effect of carbon removal and recovering the iron catalysts. For the catalytic decomposition studies, in addition to carbon black particles in the aerosol form, a layer of mirror quality highly-reflective thin film was also observed in the central region of the reaction tube as shown in Fig. 8(a). XRD analysis (Fig. 8(b)) confirmed that graphite was the major component.

4. Conclusion

The thermal and catalytic decomposition of liquid fuels were investigated in an aerosol reactor configuration to produce hydrogen and an easily separable solid carbonaceous aerosol product. The scheme is investigated as a possible route to solar driven hydrogen generation. To demonstrate this process scheme, iron was used as a catalytic material which was generated *in-situ* by thermal cracking of iron pentacarbonyl. The addition of iron catalyst was found to lower the onset temperature of fuel decomposition, and decrease the reaction activation energy. Co-injection of water vapor, which acts as a catalyst surface cleaning agent, significantly enhanced H_2 yield. The effect of fuel structure on the hydrogen yield from thermal decomposition follows the trend, alkanes > alkenes and cycloalkanes > aromatics and the overall order of hydrogen yield follows n-octane > methylcyclohexane > iso-octane > 1-octene > toluene. With the addition of iron catalyst, toluene has the highest yield enhancement by over a factor of six. The carbon black particles and graphite films were co-produced from the decomposition process.

Acknowledgment

Support for this work comes from an NSF-NIRT (EEC-0506968) grant.

REFERENCES

- [1] Navarro RM, Pena MA, Fierro JLG. Hydrogen production reactions from carbon feedstocks: fossils fuels and biomass. *Chemical Reviews* 2007;107:3952–91.
- [2] Muradov NZ, Veziroglu TN. From hydrocarbon to hydrogen-carbon to hydrogen economy. *International Journal of Hydrogen Energy* 2005;30:225–37.
- [3] Muradov NZ. CO_2 -free production of hydrogen by catalytic pyrolysis of hydrocarbon fuel. *Energy & Fuels* 1998;12:41–8.
- [4] Muradov N. Hydrogen via methane decomposition: an application for decarbonization of fossil fuels. *International Journal of Hydrogen Energy* 2001;26:1165–75.
- [5] Ahmed S, Aitani A, Rahman F, Al-Dawood A, Al-Muhaish F. Decomposition of hydrocarbons to hydrogen and carbon. *Applied Catalysis A: General* 2009;359:1–24.
- [6] Steinfeld A. Solar thermochemical production of hydrogen – a review. *Solar Energy* 2005;78:603–15.
- [7] Ma X, Zachariah MR. Size-resolved kinetics of Zn nanocrystal hydrolysis for hydrogen generation. *International Journal of Hydrogen Energy*;35:2268–2277.

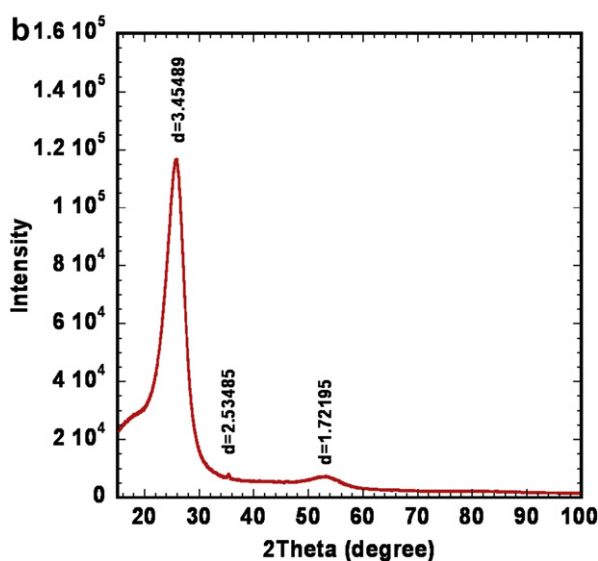


Fig. 8 – (a) Thin films collected from the wall of the reaction tube (b) XRD result of the thin film collected from the central region of the reaction tube.

- [8] Steinfeld A. Solar hydrogen production via a two-step water-splitting thermochemical cycle based on Zn/ZnO redox reactions. *International Journal of Hydrogen Energy* 2002;27: 611–9.
- [9] Weidenkaff A, Reller A, Sibieude F, Wokaun A, Steinfeld A. Experimental investigations on the crystallization of zinc by direct irradiation of zinc oxide in a solar furnace. *Chemistry of Materials* 2000;12:2175–81.
- [10] Haueter P, Moeller S, Palumbo R, Steinfeld A. The production of zinc by thermal dissociation of zinc oxide – solar chemical reactor design. *Solar Energy* 1999;67:161–7.
- [11] Dahl JK, Buechler KJ, Weimer AW, Lewandowski A, Bingham C. Solar-thermal dissociation of methane in a fluid-wall aerosol flow reactor. *International Journal of Hydrogen Energy* 2004;29:725–36.
- [12] Meier A, Kirillov VA, Kuvshinov GG, Mogilnykh YI, Reller A, Steinfeld A, et al. Solar thermal decomposition of hydrocarbons and carbon monoxide for the production of catalytic filamentous carbon. *Chemical Engineering Science* 1999;54(15–16):3341–8.
- [13] Steinfeld A, Kirillov V, Kuvshinov G, Mogilnykh Y, Reller A. Production of filamentous carbon and hydrogen by solarthermal catalytic cracking of methane. *Chemical Engineering Science* 1997;52:3599–603.
- [14] Hirsch D, Steinfeld A. Solar hydrogen production by thermal decomposition of natural gas using a vortex-flow reactor. *International Journal of Hydrogen Energy* 2004;29:47–55.
- [15] Otsuka K, Shigeta Y, Takenaka S. Production of hydrogen from gasoline range alkanes with reduced CO₂ emission. *International Journal of Hydrogen Energy* 2002;27:11–8.
- [16] Takenaka S, Kawashima K, Matsune H, Kishida M. Production of CO-free hydrogen through the decomposition of LPG and kerosene over Ni-based catalysts. *Applied Catalysis A: General* 2007;321:165–74.
- [17] Biniwale RB, Kariya N, Ichikawa M. Dehydrogenation of cyclohexane over Ni based catalysts supported on activated carbon using spray-pulsed reactor and enhancement in activity by addition of a small amount of Pt. *Catalysis Letters* 2005;105:83–7.
- [18] Kariya N, Fukuoka A, Utagawa T, Sakuramoto M, Goto Y, Ichikawa M. Efficient hydrogen production using cyclohexane and decalin by pulse-spray mode reactor with Pt catalysts. *Applied Catalysis a-General* 2003;247(2): 247–59.
- [19] Okada Y, Sasaki E, Watanabe E, Hyodo S, Nishijima H. Development of dehydrogenation catalyst for hydrogen generation in organic chemical hydride method. *International Journal of Hydrogen Energy* 2006;31:1348–56.
- [20] Wang YG, Shah N, Huffman GP. Pure hydrogen production by partial dehydrogenation of cyclohexane and methylcyclohexane over nanotube-supported Pt and Pd catalysts. *Energy & Fuels* 2004;18:1429–33.
- [21] Wang YG, Shah N, Huffman GP. Simultaneous production of hydrogen and carbon nanostructures by decomposition of propane and cyclohexane over alumina supported binary catalysts. *Catalysis Today* 2005;99:359–64.
- [22] Wang TH, Zhu YF, Jiang Q. Size effect on evaporation temperature of nanocrystals. *Materials Chemistry and Physics* 2008;111:293–5.
- [23] Karlsson MNA, Deppert K, Wacaser BA, Karlsson LS, Malm JO. Size-controlled nanoparticles by thermal cracking of iron pentacarbonyl. *Applied Physics A: Materials Science & Processing* 2005;80:1579–83.
- [24] Kissin YV. Chemical mechanisms of catalytic cracking over solid acidic catalysts: alkanes and alkenes. *Catalysis Reviews-Science and Engineering* 2001;43:85–146.
- [25] Olah GA. *Hydrocarbon chemistry*. John Wiley & Sons, Inc.; 2003.
- [26] Wojciechowski BW. The reaction mechanism of catalytic cracking: quantifying activity, selectivity, and catalyst decay. *Catalysis Reviews-Science and Engineering* 1998;40: 209–328.